Journal of Nuclear Materials 403 (2010) 32–41

Contents lists available at ScienceDirect

Journal of Nuclear Materials

journal homepage: www.elsevier.com/locate/jnucmat

Evidence for a kinetic bias towards antisite formation in SiC nano-decomposition

G. Roma *, J.-P. Crocombette

CEA, DEN, Service de Recherches de Métallurgie Physique, F-91191 Gif sur Yvette, France

ARTICLE INFO

Article history:
Received 21 December 2009
Accepted 1 June 2010

ABSTRACT

This paper is devoted to the investigation of the mechanisms of Frenkel pair recombination in cubic silicon carbide. We use first principles calculations in the framework of Density Functional Theory (DFT) and we explore a variety of possible recombination paths using constrained relaxations and the Nudged-Elastic-Band (NEB) method for various possible neutral Frenkel pairs, including those formed by defects on different sublattices (carbon and silicon). We detect several metastable configurations, some of which have not been described previously. We also consider that silicon vacancies can assume the form of carbon antisite–carbon vacancy complexes and, as such, their recombination with interstitials can occur along specific paths. In particular, in this case, we find that the recombination with silicon interstitials would probably produce antisite pairs. Finally, we use our calculated recombination barriers for a simplified kinetic model which shows that, under certain hypotheses, the annealing of irradiation defects can lead to the build up of a non negligible concentration of antisites, i.e., to a nanoscale decomposition of the material driven by a kinetic bias.

1. Introduction

Silicon carbide has promoted a long lasting scientific interest for its qualities as a high temperature material for applications in microelectronics and other fields. In the field of nuclear materials it has been used as a cladding material due to its mechanical properties at very high temperatures and its tightness with respect to fission products. However, predicting the evolution of the properties of this material under irradiation is still a hard task.

At high temperature, the evolution of defect populations leads to microstructural modifications [1,2]; probably many mechanisms are contributing to this evolution. Indeed several mechanisms have been studied from the theoretical point of view, from migration of simple vacancies and interstitials [3], to clustering of carbon interstitials [4], and other more complicated processes, in particular in order to explain the so called D_I photoluminescence, which persists at very high temperatures. At sufficiently high temperature not only interstitials but also vacancies should be mobile; furthermore, silicon vacancies should easily transform into V_C–C_{Si} complexes, which are more stable [5,3,6,7]. However no comprehensive model able to give a quantitative description of the microstructural evolutions and the formation of dislocation loops and swelling on the basis of mechanisms at the atomic scale has been established. In order to build such a model several atomic processes should be included in a higher level model, like event-based Monte Carlo [8] or rate theory. In this paper we make a first step in this direction, with a simplified rate theory model.

At low temperature, below a threshold which depends on the irradiation dose, silicon carbide is known to undergo amorphisation [9]. The structure of the amorphous produced by irradiation, both with electrons or ions, is known to contain a non negligible fraction of homonuclear bonds, up to 30% C–C and Si–Si bonds [10,11]. The detailed mechanisms leading to them is not clearly known; molecular dynamics simulations with empirical potentials of damage production [12] can give some qualitative insight, but they are questionable for a quantitative description of homopolar vs. heteropolar bonds and for the energy barriers. Indeed, at temperatures below the amorphisation threshold, interstitials should already be mobile, according to first principles calculations [3], and annealing with immobile vacancies should occur; this can lead to normal sites or to antisites. In the former case—for example a carbon vacancy with a carbon interstitial—we will speak of homogeneous recombination, in the latter—say a carbon vacancy with a *silicon* interstitial—we will qualify it as heterogeneous. The goal of this work is to treat on the same footing both classes of processes.

The recombination of close Frenkel pairs has been studied by mean of empirical potentials [13,14]; these works are certainly a valuable contribution for they take into account the distribution of recombination paths which are relevant at a given temperature, and also fully include the anharmonic contributions to atomic dynamics. However, standard empirical potentials, unable to describe charge transfer, are questionable when used to study specific atomic movements. A quantum description of the electronic density, such as in Density Functional Theory (DFT), is required in order to study in detail the annealing mechanisms of point defects. A first attempt in this direction was done by Rauls and coworkers [15]; their work was devoted to the recombination of

* Corresponding author. Tel.: +33 1 69 08 18 57; fax: +33 1 69 08 68 67.
E-mail address: roma@cea.fr (G. Roma).

0022-3115/$ - see front matter © 2010 Elsevier B.V. All rights reserved.
doi:10.1016/j.jnucmat.2010.06.001

carbon interstitials with carbon or silicon vacancies in 4H–SiC, and suggested that the recombination with V_C, leading to a normal site, had higher barrier than the one with V_{Si}, leading to a carbon antisite. This finding suggests that a kinetic bias exists towards the formation of carbon antisites The paper by Rauls, up to our knowledge, is the only one reporting on calculations of barriers for a carbon interstitial–silicon vacancy recombination mechanism, leading to an carbon antisite defect. We do not know of any work discussing the heterogeneous recombination of a silicon interstitial with a carbon vacancy.

A work by Bockstedte and coworkers [6] followed, where recombination barriers leading to perfect sites were investigated in several charged states. This paper suggests a hierarchy of annealing mechanisms, starting from the recombination of close bound Frenkel pairs, with barriers of a few 10th of an eV (similar or lower than migration barriers of the interstitials), then annealing of interstitials and vacancies due to interstitial migration, and, last, the transformation of remaining V_{Si} into V_C–C_{Si} complex. The latter picture applies to charge-compensated SiC. The Fermi level position was found to affect in an important way the hierarchy of mechanisms, as for *p*-type SiC the interstitials are much less mobile, and the metastability of the silicon vacancy is revealed at a lower temperature. Although the possibility of obtaining an antisite pair from the recombination of a tetrahedral silicon interstitial with a silicon vacancy was investigated, the case of the recombination of a split interstitial with a V_C–C_{Si} complex was not considered.

The formation of carbon and silicon interstitial clusters was also predicted [16,4,17]. The emission of interstitials from bound Frenkel pairs or from carbon interstitial clusters is considered to be a negligible mechanism due to the relatively large binding energy of those complexes.

A more recent work also dealt with recombinations of neutral Frenkel pairs giving perfect sites [18].

Very recently a combined experimental/theoretical work [19] identified a Frenkel pair in *n*-type 3C–SiC after electron irradiation. This close Frenkel pair is supposed to be in charge state +3 (a negative vacancy and 4+ tetrahedral interstitial, $V_{Si}^{-}I_{Si_{TC}}^{4+}$) and to recombine by overcoming a barrier of 2.4 eV.

None of the previously cited works used the results obtained from first principles calculations to build a kinetic model able to describe the evolution of defect populations, either at equilibrium or not (for example under irradiation). Our work makes a first step in this direction; from the first principles results for homogeneous and heterogeneous recombination barriers we build a simplified kinetic model simulating the annealing of non-equilibrium concentrations of Frenkel pairs.

In this paper we revisit the DFT approach to Frenkel pair recombination in order to establish a comparison of homogeneous vs. heterogeneous recombination; we obtain, as a by product, also the recombination distance, which is another parameter entering models for recombination rates. It proved more difficult than initially thought to give an answer to the question: *"Is there a kinetic bias towards antisite formation coming from the recombination of Frenkel pairs?*", because of the complexity of the energy landscapes. However our results provide some evidence that, in certain conditions, this bias could be an actual issue. We limit our calculations to the neutral state because the complexity of the energy landscape make these calculations computationally very demanding. Although antisites (and of course normal sites) are expected to be essentially neutral, the dominant charges of isolated vacancies and interstitials depend on the position of the Fermi level, so we do not overlook the need to investigate the recombination of charged Frenkel pairs. We stress, however, that complex charge dynamics should occur when a charged interstitial will encounter an oppositely charged vacancy. At low temperature, the effective recombination distances for some charged pairs, related to the Onsager distance [20], are too large to be treated by a first principles approach.

In Section 2 we will describe the theoretical framework and technical details, in Sections 3 and 4, we will present the results for the recombination of carbon and silicon interstitials, respectively. Section 5 is devoted to the analysis of several aspects of our results; it contains a discussion based on a simple rate theoretical model. Appendix A describes the details of the constraints used for the migration paths' searches.

2. Methods and technical details

This section, devoted to our methodological approach to the study of recombination, is split into two subsections. The first one provides the details of the DFT approach used for total energy calculations. The second one deals with saddle point search and energy landscape exploration.

2.1. Total energy calculations

Total energy calculations were performed at the DFT-LDA level, using norm conserving and ultrasoft pseudopotentials for silicon and carbon, respectively. The plane-waves cutoff was set at 30 Ry for wavefunctions and 120 Ry for the density, the latter ensuring sufficient accuracy for energy and forces. Relaxations were performed up to a force threshold of 10^{-3} Ry/Bohr, with the volume fixed at the bulk equilibrium volume. Defects, one antisite or a Frenkel pair, were introduced in $3 \times 3 \times 3$ cubic supercells of β-SiC containing 216 atoms. We found that $2 \times 2 \times 2$ cubic supercells, containing 64 atoms, were too small to model Frenkel pairs; in particular, we found that interstitials, at their largest distance from a vacancy in the supercell, were not assuming the expected equilibrium position and the binding energies were still very high. Following a recent work on silicon interstitials [21], whose convergence with supercell size proves to be very difficult, we assume that our 216 atoms supercell, with the Brillouin Zone (BZ) sampled by a $2 \times 2 \times 2$ shifted Monkhorst–Pack mesh, gives results which are reasonably converged. Even if formation energies still suffered errors as large as for the silicon interstitial (0.2 eV [21]) the error on barriers should be definitely lower. The errors coming from performing fixed volume calculations are relatively small as the residual pressures are never larger than 0.8 GPa (absolute values) for homogeneous recombinations and 2.5 GPa for heterogeneous ones.

We show, in Table 1, a comparison of formation energies in the $2 \times 2 \times 2$ and $3 \times 3 \times 3$ supercells for antisites, which are the end point of heterogeneous relaxations. In this case the formation energies are relatively well converged even for the $2 \times 2 \times 2$ supercell. The calculations were performed using the Quantum-Espresso package [22].

2.2. Energy landscape exploration

The search for saddle points and, more generally, for minimum energy paths in the multi-dimensional space representing the configuration of tenths or hundreds of atoms is particularly demanding when the basic unit, i.e., one total energy calculation, is done at the quantum level.

Table 1
The formation energy of antisites in SiC for two supercell sizes (containing 64 and 216 atoms respectively); the last column shows the residual pressure.

Antisite	Supercell	E_f (Si-rich) [eV]	E_f (C-rich) [eV]	ΔP [GPa]
C_{Si}	$2 \times 2 \times 2$	3.96	3.04	−4.1
C_{Si}	$3 \times 3 \times 3$	3.88	2.96	−1.7
Si_C	$2 \times 2 \times 2$	3.36	4.28	4.5
Si_C	$3 \times 3 \times 3$	3.19	4.12	0.8

Recently the Nudged-Elastic-Band (NEB) [23] method for calculating saddle point energies has been widely used. It consists in constructing a certain number of intermediate configurations (NEB images) between an initial and a final state (a migration path) and then relaxing the whole path by minimising a function which includes not only the energy of each configuration in the path, but also the energy of fictitious springs connecting the NEB images in configurational space of dimension $3N$ (N = number of atoms).

We remind here that, in a complex energy landscape as the one we are going to explore, the possible paths and saddle points connecting an initial and a final point are multiple, several valleys can be followed and, approaching to the ridge, several waypoints can be found to a neighbouring valley. Mentioning this complexity is not at all a trivial general reminder, but reflects a real issue that we faced searching for recombination paths, as it will be seen in the following. A saddle point, outcome of a path relaxation according to the NEB procedure, depends on the choice of the initial path, which is in general a linear interpolation between the initial and final point. In order to avoid this bias, in several cases we started from a normal site or an antisite and searched for a Frenkel pair configuration without imposing it, also because the most favourable Frenkel pair configuration is not known a priori when the defects are still close and interacting with each other. This justifies the second method that we used, which is exposed in the following.

The fictitious springs of the NEB procedure act as restraints on intermediate positions in order to prevent them to fall to the bottom of the potential well, the local minimum. Instead of restraints, holonomic constraints can be used in order to build minimum energy paths, and indeed have been used at least since the pioneering proposal by Bennett [24]. In order to find a saddle point any one-dimensional constraint of the form

$$g(\{\mathbf{r}_i\}_{i=1,N}) = 0 \tag{1}$$

can be used, like a distance between two atoms or a bond angle. The one that we used, which is a generalisation of the constraint originally proposed by Bennett for the migration of a vacancy in an fcc (face centered cubic) lattice, is described in Appendix A. The connection, and similarity, with the so called "drag method" is also clarified in Appendix A, which justifies that in the following we use the expression "dragging" or "pushing" an atom.

Successive constrained relaxations allow to build a minimum energy path between two minima even when one of them (the final point) is not known a priori. This is clearly an advantage with respect to the NEB method. Moreover, in some cases, a number of constrained relaxations can be less demanding than a single NEB calculation, or can avoid some electronic convergence problems related to the choice of the initial path, which is usually chosen as a linear interpolation between the initial and final state, in configurational space of dimension $3N$ (N = number of atoms). Indeed we encountered this difficulty when trying to do a NEB calculation between a distant I_C–V_C pair in a 216 atoms supercell and one with no defects. Another possibility would be to search for intermediate shorter NEB paths between stable positions, but the choice of intermediate positions would bias the overall path.

We compared NEB and our constrained relaxation procedure for the recombination of a silicon interstitial with a carbon vacancy in a 64 atoms supercell; starting by a silicon antisite we progressively moved the silicon atom away from the vacancy and performed successive constrained relaxations. From the final path, whose steps are not equispaced in $3Nd$, a set of equispaced images was obtained by interpolation and used as a starting point for a NEB calculations. The results for the two methods are compared in Fig. 1. The recombination barrier, in this case, depends on the direction in which the antisite atom is pushed. The NEB results are in very good agreement with the constrained relaxations, as expected, underlining the dependence of the NEB results on the starting path.

For this reason we searched for paths by pushing the jumping atom in two directions ($\langle 1\,1\,1\rangle$ and $\langle 1\,1\,0\rangle$) in order to check different valleys for most of the Frenkel pair recombinations presented in the following. We used, in some cases, refined procedures allowing to adjust the constraint at each migration step by using the information from previous migration steps. These improvements are described in Appendix A (formulas (12) and (13)). In several cases we also performed NEB calculations between intermediate configurations, mostly using the climbing image technique, in order to check for the presence of a barrier between two points.

3. Carbon recombination with vacancies

In order to study the annealing of vacancies through recombination with carbon interstitials we started from a normal site and from a carbon antisite and, in both cases, we pushed the carbon atom, through successive constrained relaxations, to a distance between 0.5 and 0.6 nm, until we could find a stable position. Let us discuss first the results for the first case, the homogeneous recombination.

3.1. Homogeneous carbon recombination

The calculation of the path for the homogeneous recombination lead us to some configurations where the electronic convergence was very slow or not attainable. In order to overcome this problem we had to reduce the step between constrained relaxations and to use the procedure described by formula (13) of Appendix A. We also checked by further NEB and constrained relaxation calculations. The result obtained by starting from the perfect crystal and ejecting a carbon atom from its site is the curve C_C-constr2 in Fig. 2. We underline that the unconstrained relaxations of the last five points of this curve lead all to point p_1. We found, however, through interpolation and unconstrained relaxation, other minima. From one of these (p_2 in figure) we also built a backward path, from Eq. (13). These points are shown as filled circles in Fig. 2. As a check we performed NEB calculations with a climbing image between the starting point and the two intermediate, fully relaxed, points p_1 and p_2. The outcomes are shown in the insets of Fig. 2, confirming the barriers of 0.2 eV between p_1 and the perfect crystal (p_0) and of

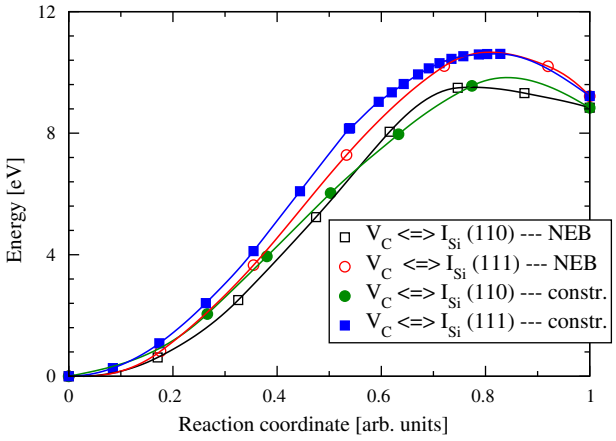

Fig. 1. Comparison of energy profiles for $I_{Si} \rightleftharpoons V_C$ recombination in a 64 atoms supercell obtained with NEB or with constrained relaxations. The reaction coordinate is, for both, the distance in $3Nd$ normalised to the $3Nd$ distance between the first and last point. For each method we show the recombination in two different valleys, one corresponds to pushing the antisite atom in the $\langle 1\,1\,1\rangle$ direction, and the other along $\langle 1\,1\,0\rangle$.

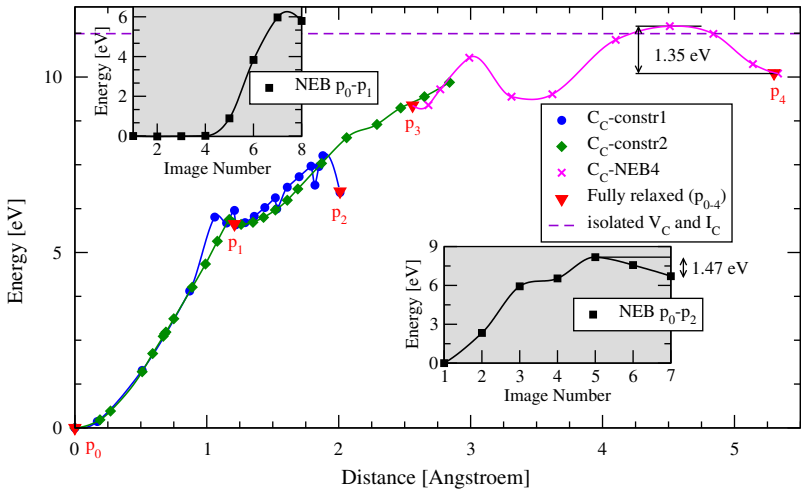

Fig. 2. Recombination energy profiles for a carbon interstitial with a carbon vacancy. Curves CC-constr 1 and CC-constr 2 in the main panel have been obtained by constrained relaxations, the diamonds by ejecting a carbon atom from its normal site, the circles by starting from point p_2 and going backward. CC-NEB4 are points from a NEB calculation. The x-axis represents the distance in $3N$ dimensions with respect to p_0, which is approximately the one in 3D between the interstitial and the vacancy when they are far enough from each other. The two insets represent the energy profiles of NEB calculations to go from p_0 to p_1 (upper left) and from p_0 to p_2 (lower right). Lines are splines interpolations.

1.47 eV between p_2 and p_0. The position p_2 resembles a close pair of carbon and silicon dumb-bells, or a distorted antisite pair, and is still much higher in energy than the antisite pair. In order to reach a larger distance between the interstitial and the vacancy, we selected some configurations out of several ones obtained by constrained relaxation (not shown in Fig. 2) and performed NEB calculations between them. The curve CC-NEB4 in Fig. 2 is one of them; it shows that the migration of a carbon interstitial from a second nearest neighbour site to the vacancy, to a fourth nearest neighbour one involves a migration energy around 2 eV, which is much higher than the one for an isolated interstitial ($\simeq$0.5 eV). The opposite transformation, from fourth to second nearest neighbour, involves a barrier of 1.35 eV, close to the one to recombine from point p_2. We should remark here that, while point p_3 has indeed been found by a fully unconstrained relaxation, the energy barrier separating it from the closest point on the curve C_C–constr2 is less than 0.1 eV.

3.2. Heterogeneous carbon recombination

We pursued our study by calculating the path from a carbon antisite, C_{Si}, to a distant V_{Si}–I_C pair. We show in Fig. 3 the energy profiles for two recombination paths.

The recombination path C_{Si}-path1 (diamonds) has been obtained by the constrained relaxations procedure along the $\langle 1\,1\,0\rangle$ direction; a similar procedure along the $\langle 1\,1\,1\rangle$ direction led to a higher barrier (2.6 eV). We complemented the constrained relaxations by a NEB calculation which allowed to refine the barrier and to find the dip bottoming out at π_3. This latter point corresponds to a silicon vacancy still bound to a distorted carbon interstitial which finds its equilibrium structure as a carbon trimer.

To lead to it we started with a carbon antisite and pushed on one of the surrounding carbons—not onto the antisite itself—in order to avoid producing a carbon–carbon exchange. One could suppose that ejecting a carbon atom neighbouring the carbon on the silicon site would produce a carbon vacancy, leaving the carbon antisite as it is. In fact this is not the case. The carbon on the silicon site follows the pushed first neighbour, leaving a silicon vacancy. It is thus interesting to remark that, along the path, the silicon vacancy does not transform into a V_C–C_{Si} complex. Path C_{Si}-path1 finally leads to a genuine I_C–V_{Si} pair, point π_4 in Fig. 3.

The highest barrier for the recombination along this path is the one between π_3 and π_0, approx. 1.25 eV, slightly lower than the one for homogeneous recombination.

Here again the complexity of the energy landscape led us to discover a further minimum, π_2. This configuration involves, on one side, a carbon trimer (a distorted C_{Si}), on the other side a complex collective distortion where one cannot identify neither a silicon vacancy, nor a V_C–C_{Si} complex, into which the former could transform [5,3,6]. The path C_{Si}-path2 (triangles) in Fig. 3 is built by two NEB calculations between fully relaxed points π_{0-2}. For this path we can observe a very small barrier around 0.15 nm separation and a larger one, 0.8 eV, at larger distance, between 0.3 and 0.4 nm. The point indicated as π_1 in the figure corresponds to a collective distortion of the carbon antisite where one of the carbon atoms surrounding the antisite has migrated to form a dumbbell with a carbon atom not participating to the antisite structure. The final point π_2 includes a tri-coordinated carbon, that resembles the sp^2 structure of the V_C–C_{Si} complex, and three tri-coordinated silicon atoms. The interstitial side has a trimer structure. The fact that π_2 is very similar to a Frenkel pair whose vacancy side has the V_C–C_{Si} structure explains why its energy is lower than the sum of the formation energies of a carbon interstitial and a silicon vacancy (indicated by the dashed-line in Fig. 3). We consider this path the preferred one for the recombination of a carbon interstitial with a V_C–C_{Si} complex.

4. Silicon recombination with vacancies

We applied, for the recombination of silicon interstitials with vacancies, the same procedures as for carbon. We do not address here the problem of the charge state of silicon interstitials, which carries some difficulties which are inherent to DFT in the standard semilocal formulation [21]; we treat here only the neutral state as we start from a normal site or a silicon antisite which are both expected to be neutral.

4.1. Homogeneous silicon recombination

The recombination of a silicon interstitial with a silicon vacancy in the neutral state has been studied previously [6,18]. In particular, a concerted motion of silicon atoms with very low barrier

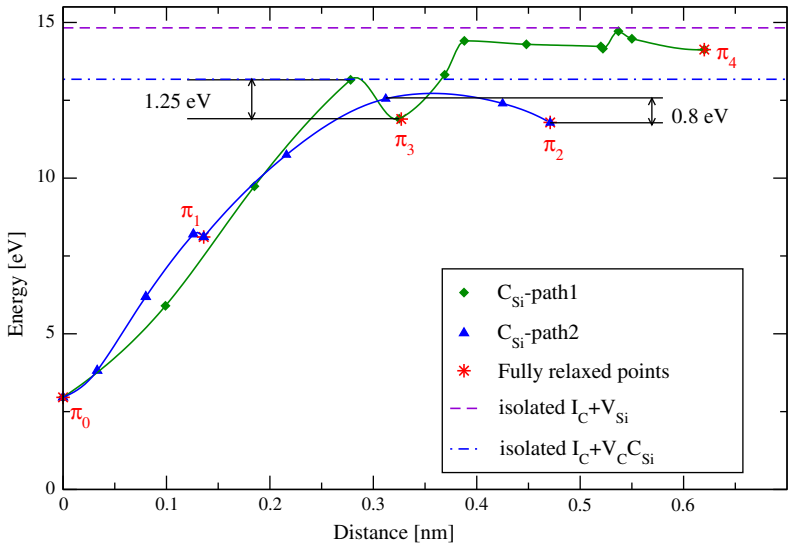

Fig. 3. Two energy profiles for the recombination of defects leading to a carbon antisite (π_0). Energies refer to C-rich conditions. The green curve (diamonds) represents the recombination of a well separated I_C–V_{Si} pair (point π_4). The intermediate dip, point π_3, contains a silicon vacancy and a carbon trimer. The blue curve (triangles) represents two different NEB calculations, forming a path through the fully relaxed points π_0–π_2, marked by red stars. π_2 is a complex distorted configuration not easily identifiable with known defects. (For interpretation of the references to colour in this figure legend, the reader is referred to the web version of this article.)

(0.2 eV) [3] was found for the recombination in the neutral state. We reproduced this mechanism finding an even lower (0.03 eV) recombination barrier. However, we further explored the possible recombination paths without imposing this collective movement; starting from a silicon atom on a normal site we displaced it through successive constrained relaxations.

The ejection of a silicon atom from a normal site produces modifications on the network of silicon carbide which are more spectacular than for carbon. The silicon is the largest atoms between the two and is expected to produce larger distortions. Moreover, it is known that the silicon vacancy is metastable, in β-SiC, for Fermi energies from 0 to 1.5 eV above the valence band top (VBT) [3,6] (which covers the whole DFT band gap); beyond it (n-doping conditions) V_{Si} would be the ground state according to calculations. Its stable form in p and intrinsic conditions is the C_{Si}–V_C complex. The barriers separating the two configurations, as reported in Ref. [6], range from 6.1 to 2.4 eV (V_C–$C_{Si} \rightarrow V_{Si}$, charges +2 to −1) and from 1.9 to 2.7 eV ($V_{Si} \rightarrow V_C$–C_{Si}, charges from +1 to −2). Indeed we found, along the recombination path, a configuration where we can recognise a carbon antisite, however the first steps of the silicon atom leaving its normal site leads to an antisite pair, which provides a relatively deep trap. This structure, which is shown in Fig. 4, corresponds to the fully relaxed point P_3 at 0.16 nm in the left panel of Fig. 5.

The antisite pair configuration, and the barrier for its recombination, has been previously studied by first principles calculations [25,26]. Its structure was not described in details in previous studies, for this reason we present it in Fig. 4; it is formed by two pyramids, one made by carbon and the other by silicon atoms; the basis is, for both, an equilateral triangle with side 0.275 nm for carbon and 0.340 nm for silicon; the edge is 0.163 nm for carbon and 0.218 nm for silicon. The Si–C bond connecting the two pyramids by their apices amounts 0.185 nm, which is slightly compressed with respect to the Si–C bond length in the perfect bulk (0.188 nm). One can look at this structure as two interpenetrating tetrahedra, one formed by three silicons and one carbon and the other by three carbons and one silicon. Both tetrahedra are regular ones (dihedral angles of 70°). As far as we know, it was not recognised that the antisite pair could provide an intermediate state for the recombination of a silicon Frenkel pair. To check the relevance and depth of this dip during recombination we performed two NEB

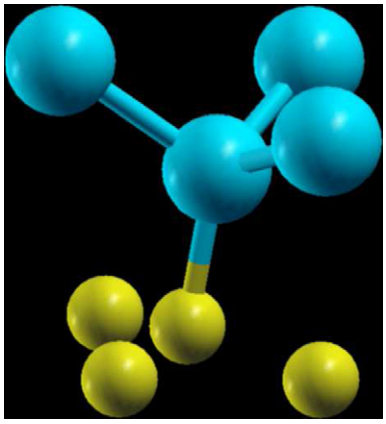

Fig. 4. The basic building block of the structure of the antisite pair in cubic silicon carbide (point P_3 in Fig. 5). Larger atoms are silicons, smaller ones are carbons.

calculations (paths Si_{Si}-NEB1, from P_1 to P_3, and Si_{Si}-NEB2, from P_1 to P_4); both paths show similar qualitative behaviour, even if they do not pass through exactly the same saddle point. The lowest barrier that we found for escaping the antisite pair trap is 3.12 eV, in agreement with previous results [25,26].

Pushing further the silicon side of the antisite pair (path Si_{Si}-constr1) leads to a metastable configuration including an sp^2 carbon atom bound with three others (P_4), which reminds of the structure of the C_{Si}–V_C complex. However here the silicon interstitial is still relatively close (0.3 nm) to the normal site where it came from. Then, up to a relatively distant pair configuration (>0.6 nm), no other barrier than the normal migration one seems to occur. Indeed this barrier is comparable to the one that we recently found for the migration of the silicon interstitial in the neutral state [21]. In this part of the path, and in particular at the local minima P_5–P_7, the structure of the vacancy side still contains the sp^2 carbon structure typical of the C_{Si}–V_C complex. This is almost certainly the explanation why the P_6 configuration, which includes an $I^{Si}_{sp\langle 1\,1\,0\rangle}$ interstitial, is lower in energy by 1.4 eV than the Frenkel pair that recombines with the concerted motion, previously mentioned. The latter Frenkel pair includes a silicon vacancy and an $I^{Si}_{sp\langle 1\,1\,0\rangle}$ at the

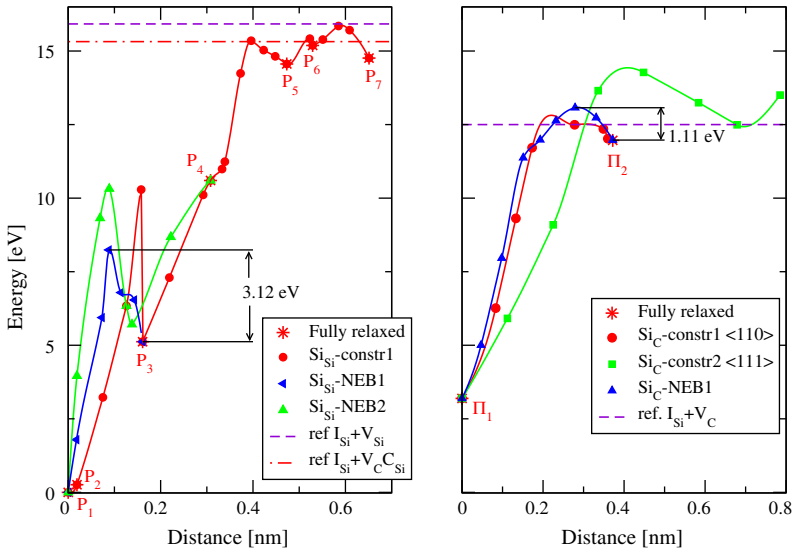

Fig. 5. Recombination energy profiles for silicon interstitials with a V_C–C_{Si} complex (left panel) and with a carbon vacancy (right panel). The energies in the latter refer to Si-rich conditions. Triangles refer to points obtained from NEB calculations. Stars represent fully relaxed points (i.e. local minima). Lines are spline interpolations. Further details concerning the constrained relaxations are in the text.

same distance as the one in P_6, although the orientation of the interstitial relative to the line connecting the interstitial and the vacancy (I–V) is not the same: for the interstitial recombining through the concerted motion the orientation is along the I–V line, while in P_6 the split interstitial is perpendicular to it.

4.2. Heterogeneous silicon recombination

The heterogeneous recombination of a silicon interstitial with a carbon vacancy occurs along smoother profiles. As for the carbon heterogeneous recombination, the barrier obtained through a Bennett constraint along ⟨1 1 1⟩ is higher than along ⟨1 1 0⟩. The profiles are shown on the right panel of Fig. 5, paths Si_C-constr2 and Si_C-constr1 respectively. The path along ⟨1 1 0⟩ was checked with a NEB calculation on nine images, which led to a slightly higher barrier, of 1.11 eV (path Si_C-NEB1 on the figure). The final configuration, Π_2, is clearly identifiable as a distant I_{Si}–V_C pair, with a split silicon interstitial configuration along the ⟨1 1 0⟩ direction.

5. Discussion

5.1. Complexity of the energy landscape

The first inevitable remark concerns the complexity of the energy landscape that we found. The assumption, ordinarily made in binary metallic alloys, that recombination barriers, at least those leading to normal sites, are not higher than migration barriers, is clearly not justified here. Moreover our calculations—not only the points shown in the previous figures, but also other path segments—show that the energy landscape is very noisy, presenting several local minima and, consequently, a large variety of paths connecting them. We are thus aware that our sampling is only very partial; however, it can highlight some major features. For example, in the case of the recombination of a silicon interstitial with a V_C–C_{Si} complex (Fig. 5, first panel) the three curves, although describing different paths, all show a trapping in the basin bottoming out at the antisite pair. The different height of the saddle points for antisite pair recombination reminds us that a full statistical sampling of available paths should in principle be performed in order to allow an evaluation of energy and entropy factors which are limiting recombinations. This is out of reach of the present approach. We also remark that an evaluation of jump entropy factors based on vibrational modes at the saddle point (which we also neglect) would be unable to take into account the variety of paths, between the same initial and final state, which are separated from each other by ridges on a smaller energy scale.

5.2. Comparison with previous results

The only published work attempting a comparison of homogeneous and heterogeneous recombination, as we previously mentioned, is the one by Rauls [15], using a DFT based tight-binding method. It should be stressed that their approach, relying on a minimal basis set of localised orbitals (only s and p), poorly describes the conduction band. The high migration barrier for the carbon split interstitial that was reported in that paper (almost 3 eV, much higher than the DFT result of 0.5 eV [3]) is probably a direct consequence of this approximation. A similar effect of the basis set has been shown for some neutral configurations of the silicon interstitial [21]. Of course one could argue that an accidental widening of the band gap due to an incomplete basis set could produce results which are more realistic than with a converged DFT calculation, as it happens for the band gap [27], but this still appears as a speculative argument.

Rauls and coworkers, dealing with neutral Frenkel pairs, report a large barrier, around 4 eV, for the homogeneous carbon recombination starting from a fourth neighbour, which is at a distance of approximately 0.37 nm. The complexity of the landscape that we found and the few details about the path given in that paper do not allow a thorough comparison with our results, however we think that the high value of their barrier is probably due to the same limitations of the tight binding model that we just mentioned for the migration of a carbon interstitial. The barrier for the second neighbour recombination (0.5 eV) is slightly higher than that of Bockstedte and coworkers [6] (0.4 eV) which is itself higher than ours (0.2 eV). The difference between the last two figures depends probably on supercell size and/or **k**-point sampling. Lucas and Pizzagalli [18] obtained a barrier of 1.24 eV for a fourth neighbour (d = 0.37 nm) recombination and one of 1.43 eV for a closer pair, as far as we understand a third neighbour recombination, with a mixed split interstitial. The latter configuration, in spite of a similar value for the recombination, does not resembles to our point p_2.

The same authors also found a lower recombination barrier (0.65 eV) for a fifth neighbour recombination.

For a heterogeneous recombination, giving a carbon antisite, Rauls found a smaller barrier, around 1 eV, starting from a third neighbour site. In this case the barrier is close to our results, which amounts to 1.25 eV or 0.8 eV, depending on the structure of the vacancy.

Let us now come to the recombination of silicon interstitials with vacancies. Here the discrepancy between the two previous works coping with it is more evident. On one side Bockstedte and coworkers [6] found a very small (0.2 eV) barrier for the recombination of a split interstitial with a vacancy in the neutral state. For the interstitial in the tetrahedral configuration, they found that it would transform into an antisite pair. Lucas and Pizzagalli [18], for the tetrahedral interstitial, found barriers of 1.84 eV or 1.05 eV according to the distance, but they do not mention the antisite pair. It should be stressed that the corresponding paths were outcomes of calculations of threshold displacement energies by molecular dynamics simulations of low energy recoils [28], which could perhaps explain the higher barriers. In both the mentioned works the vacancy was in its metastable state, i.e., a true silicon vacancy and not the V_C–C_{Si} complex.

As for our results, on the one hand we found a result similar to Bockstedte and coworkers, by imposing a collective motion of the silicon atoms in a split interstitial, as they did. Our barrier is even lower (0.03 eV). On the other hand we found that paths for the recombination of a split interstitial with a V_C–C_{Si} complex involve the passage through the antisite pair, which constitutes a deep trap. The barrier that we found for the recombination of the antisite pair is in agreement with previous works [25,26]. As far as we know the annealing of the V_C–C_{Si} complex by interstitials, carbon or silicon ones, has not been not considered previously.

Our results suggest that if the silicon vacancy, for whatever reason, has undergone the transformation to the V_C–C_{Si} complex, then its annealing by recombination with silicon interstitials would probably lead to antisite pairs. Even if in a displacement cascade silicon atoms knocked out of their sites leave behind genuine silicon vacancies, one can expect that some of them can assume the V_C–C_{Si} structure, due to the thermal spike effect of the cascade. in this case their annealing by interstitials would lead to antisite pairs.

5.3. Electronic effects and the band gap problem

As explained we chose to limit ourselves to the recombination of neutral pairs. This can include not only pairs of neutral defects, but also pairs of oppositely charged defects, say, for example, V_{Si}^{-}–I_{Si}^{+}. The effectiveness of a given recombination channel depends, in thermal equilibrium, on the products of the concentrations of the defects involved, at a given temperature and doping level, and on their mobility and recombination barrier. Even if we knew all the possible formation, migration and recombination energies the task would not be a simple one. Our specific focus here is silicon carbide under irradiation. Here concentrations are not the equilibrium ones, and initial doping conditions can be modified by irradiation defects [29]. However, in order to have an idea of how doping conditions can affect the applicability of our results, let us assume that we are in local charge equilibrium, that is the ratio of concentrations of the various charge states of a defect is the equilibrium one. Using the charge transition levels published by Bockstedte [3], we find that, according to dominant charge states, the neutral recombination should be dominant in the following Fermi energy ranges:

- V_{Si}–I_{Si}: from 0.6 to 1.1 eV above VBT (as V_{Si}^{-}–I_{Si}^{+}) and from 1.18 to 1.24 (as V_{Si}^{--}–I_{Si}^{++}), i.e., essentially in p and intrinsic conditions.
- V_C–I_C: from 1.1 to 1.8 eV above VBT (as V_C^0–I_C^0), intrinsic and moderate n conditions.
- V_{Si}–I_C: from 0.6 to 0.8 eV above VBT (as V_{Si}^{-}–I_C^{+} or V_{Si}^{--}–I_C^{++}), p conditions.
- V_C–I_{Si}: from 1.1 to 2.04 eV above VBT (as V_C^0–I_{Si}^0), i.e., intrinsic and n conditions.

Concerning the recombinations involving the V_C–C_{Si} complex, which is expected to be neutral only for $E_{Fermi} > 1.79$ eV, we can state that they occur dominantly in the neutral state only for n-type conditions.

We cannot avoid stressing, at this point, that charge transition levels above the DFT band gap (which we calculate at 1.35 eV), are certainly questionable. For this reason we checked the variation of the last occupied defect state (HOMO) along our recombination paths. This can give some hints on electronic effects during recombination, although we are aware that the complexity of charge dynamics for two defects approaching each other from large distances is out of the scope of this paper; it should certainly be addressed in the future.

We remind that not only normal sites but also antisites, one of the extremities of our recombination paths, are predominantly in the neutral state in a very large range of Fermi energies.

In the case of the homogeneous carbon recombination, along curves C_C-constr1, C_C-constr2 and C_C-NEB4 the HOMO stays inside the DFT band gap, except at the saddle point between p_3 and the following basin (i.e., the first saddle of the curve C_C-NEB4). As the carbon vacancy is expected to be positively charged for p-type and intrinsic SiC [3], it is not surprising that, once far enough from the interstitial, it can release an electron. Or, conversely, that when a positively charged vacancy is approached by a neutral interstitial the recombination can be enhanced by the capture of an electron.

In the case of both curves presented for the heterogeneous carbon recombination the HOMO stays well inside the DFT band gap, at least 0.2 eV below the conduction band edge. This would suggest that the pair can remain neutral during the recombination, at sufficiently low temperature. However, according to calculated charge transition levels [3], for an intrinsic material one would expect the dominant charged states to be V_{Si}^{-} and I_C^0, so that this recombination channel is probably not the dominant one if one assumes local equilibrium of charge states.

In the case of homogeneous silicon recombination, during the concerted motion leading to a very easy I_{Si}–V_{Si} annihilation, the last occupied electronic level is well inside the band gap. Conversely, in the case of the recombination described by the curve Si-constr1 in Fig. 5, for all the configurations for which the pair distance is larger than 0.4 nm the last occupied orbital falls into the conduction band. This suggests that the ejection of a silicon atom from its normal site, when leaving a C_{Si}–V_C complex, would probably induce a release of electrons in the conduction band, or that the recombination of a silicon interstitial with a C_{Si}–V_C complex is expected to be enhanced by the capture of electrons.

Let us now, finally, comment on the position of the last occupied defect level during the heterogeneous silicon recombination, path Si_C-NEB1 on the right panel of Fig. 5. The Fermi energy gets hybridised with the conduction band at the fourth and sixth points of this path. The starting point (Si_C) has a defect level at 0.23 eV and the final Frenkel pair has one at 1.05 eV (both referred to the VBT). Again, here, the capture of an electron during the recombination could facilitate the annealing of the pair.

5.4. A simplified model of recombination kinetics

In order to summarise, we show in Table 2 the relevant barriers for the interstitial/vacancy pair recombinations in SiC together with the recombination distances, r_0.

Table 2
Relevant barriers and recombination distances in silicon carbide for neutral Frenkel pairs, leading to normal sites or antisites. E^* is the recombination barrier, E^{mig} is the interstitial migration barrier (lower than for the vacancy), r_0 is the recombination distance.

Recombination	V_C	V_C–C_{Si}	V_{Si}
I_C	E^* = 1.35 eV E^{mig} = 0.5 eV r_0 = 0.21 nm	E^* = 0.8 eV E^{mig} = 0.5 eV r_0 = 0.47 nm	E^* = 1.25 eV E^{mig} = 0.5 eV r_0 = 0.33 nm
I_{Si}	E^* = 1.11 eV E^{mig} = 0.8 eV r_0 = 0.37 nm	E^* = 3.12 eV E^{mig} = 0.8 eV r_0 = 0.16 nm	E^* = 0.03 eV E^{mig} = 0.8 eV r_0 = 0.63 nm

These data can be used to calculate time (and temperature) dependent recombination rates for species A and B, $k(A–B, T, t)$, according to the approximate formula proposed by Waite [30]:

$$k(A{-}B,T,t) = -4\pi r_0 D \frac{s\left[1+(\pi\tau)^{\frac{1}{2}}\right]}{1+(s+1)(\pi\tau)^{\frac{1}{2}}} \tag{2}$$

where r_0 is the recombination distance, D is the sum of the diffusion coefficients of the two species, τ is a rescaled time ($\tau = Dt/r_0^2$), and s depends on the recombination and migration energies according to $s = \exp\left(\frac{E_{mig}-E^*}{k_B T}\right)$. Using rates calculated with Eq. (2), we can build a model of homogeneous kinetics, based on the following set of differential equations :

$$\frac{dC_{I_j}}{dt} = -\sum_{I\equiv Si,C} k(I_j{-}V_I,T,t) C_{V_I} C_{I_j} \tag{3}$$

$$\frac{dC_{V_j}}{dt} = -\sum_{I\equiv Si,C} k(I_I{-}V_j,T,t) C_{V_j} C_{I_I} \tag{4}$$

where the index j indicates silicon or carbon, giving then four coupled differential equations for the evolution of the four interstitial and vacancy concentrations: C_{I_C}, C_{V_C}, $C_{I_{Si}}$, $C_{V_{Si}}$.

This model is certainly oversimplifying the evolution of the concentrations of point defects, namely because it is neglecting the clustering of carbon [16,4] and silicon atoms [17] which are expected to play a non negligible role. Moreover, as it can be seen from Eq. (4), antisite pairs are not treated as an independent defect type; this is a further simplification of the model. However, it will help us to draw qualitative conclusions about the bias introduced by recombination barriers into the relative concentrations of native defects, namely antisites, under irradiation. Let us start for example with initial Frenkel pair concentrations much higher than equilibrium ones, and let these concentrations evolve according to Eqs. (3) and (4), mimicking a post-irradiation anneal. We consider here that the initial concentration of antisites is null (or negligible). We will consider two cases: in the first the silicon vacancies initially present are in their undistorted metastable form, in the second one they are in the most stable form of V_C–C_{Si} complex.

In the first case the homogeneous silicon recombination occurs quite easily. As a consequence we can observe, as shown in the upper panel of Fig. 6, that, at first, silicon vacancies and interstitials start to recombine with each other. The formation of antisites is due to the fact that silicon interstitials can also recombine with carbon vacancies, but their concentration is more than three orders of magnitude lower than the initial concentration of Frenkel pairs. When silicon interstitials are not anymore available (i.e., when their concentration gets lower than that of Si_C antisites) the concentration of vacancies stalls, showing a plateau, until they start to get annealed by carbon interstitials, forming C_{Si} antisites (light blue filled squares). Almost at the same time carbon vacancies and carbon interstitials begin to anneal each other (indeed the two processes have similar recombination barriers, 1.25 and 1.35 eV respectively).

Let us consider now the second case: here silicon interstitials preferentially anneal carbon vacancies, because the annealing of the V_C–C_{Si} complex is hindered by the large recombination barrier of antisite pairs. But also carbon antisites are more easily formed than perfect sites, as the barrier for heterogeneous recombination is only 0.8 eV, in this case. Thus, a build up of C_{Si}, then of Si_C antisites, is observed up to a concentration comparable to the initial concentration of Frenkel pairs. The fact that C_{Si} and Si_C concentrations end up at the same value is determined, in our model, simply

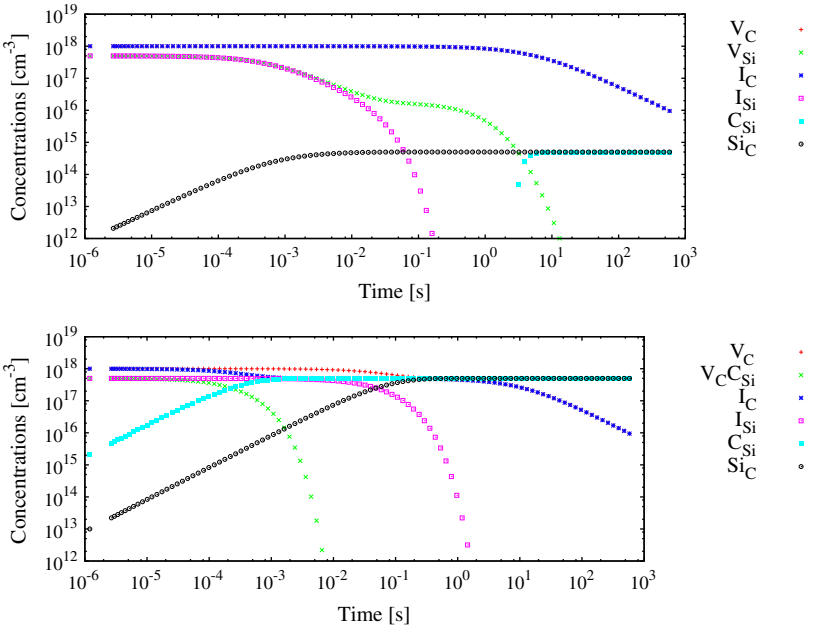

Fig. 6. The time evolution of a given initial concentration of silicon and carbon Frenkel pairs in SiC by diffusion and recombination as described by rate Eqs. (3) and (4), using the recombination barriers in Table 2. The temperature is T = 700 K. The upper panel refers to a case were silicon vacancies are in their metastable structure, and V_{Si}–I_{Si} recombination occurs with almost no barrier. The lower panel illustrate the case where vacancies take the most stable form of V_C–C_{Si} complexes, and the recombination with silicon interstitials is hindered by the antisite pair trap.

by the conservation of the stoichiometric ratio. Later the carbon interstitials which are left (more or less half of the initial concentration) achieve the annealing of carbon vacancies.

The example that we have just described suggests that the details of the structure of the defects can not only affect deeply the kinetics during recombination, but that, given the interplay of available defect species, the kinetical parameters alone can lead to a relevant accumulation of antisite defects. It goes without saying that the larger the number of defect species taken into account, the more difficult it will be to predict what would happen through a simple comparison of energy barriers. Moreover many energy barriers are still unknown, like, for example, those for clustering of silicon or carbon interstitials. A crucial problem is of course the one of the recombination of charged defects. In many cases, in silicon carbide, charged defects are supposed to have larger migration energies than neutral ones [3]; in particular the $I^{4+}_{Si_{TC}}$ interstitial, supposed to be dominant for *p*-type SiC, has a large migration energy. As for the recombination, recent findings indicate a barrier of 2.4 eV for homogeneous silicon recombination in charge state 3+ [19]. These facts would contribute to slow down the homogeneous silicon recombination. However one should be careful to conclude, even qualitatively, in this direction, because enhanced migration mechanisms for silicon interstitials, similar to Bourgoin ones [31], could be relevant for intermediate charge states, and indeed there are some experimental indications that such phenomena are present in SiC [32].

6. Conclusions

In summary, we explored several paths for the recombination of silicon and carbon interstitials with carbon and silicon vacancies in silicon carbide in the neutral state with DFT-LDA. We considered, on the same footings, recombinations giving rise to perfect sites and those leading to antisites. We highlighted an unexpected complexity of the energy landscape, with a variety of local minima and paths connecting them. Our results indicate that a substantial kinetic bias could provoke the formation of antisites when silicon vacancies assume the structure of the carbon antisite–carbon vacancy complex, which is their most stable configuration in *p*-type and intrinsic conditions. In order to illustrate this fact we proposed a simplified model of recombination kinetics based on coupled differential equations for the evolution of defect concentrations, and we applied it to a case study mimicking the post-irradiation anneal of given concentrations of Frenkel pairs.

Acknowledgements

We thank Georges Martin, for the initial suggestion he gave us to investigate about kinetic biases in the recombination of Frenkel pairs, and Thomas Jourdan, for useful help about the kinetic model. We acknowledge HPC resources from CCRT and CINES computing centres through GENCI Grant No. 2009-GEN6018. This work was carried out within the framework of the European Fusion Development Agreement (EFDA) Fusion Materials Modelling Programme.

Appendix A. Constraints for saddle point search

The method originally proposed by C.H. Bennett for searching saddle points consisted in performing molecular statics under a specific suitable constraint. For the jump of a vacancy in an fcc lattice he proposed to constrain on a given direction **d** (the jump direction) the projection of the following vector:

$$\mathbf{v} = \mathbf{r}_1 - \frac{1}{4}(\mathbf{r}_2 + \mathbf{r}_3 + \mathbf{r}_4 + \mathbf{r}_5) \tag{5}$$

where $\mathbf{r}_1$ is the position of jumping atom and $\mathbf{r}_{2-5}$ are those of four neighbouring atoms forming a "gate", through which the jumping atom is expected to pass. The constraint is then expressed by $\mathbf{v}\cdot\mathbf{d} - B = 0$, B being a constant. The second term in (5), the centre of mass of the atoms forming the gate, prevents the rigid shift of the supercell when pushing on one atom. It is easy to generalise this constraint for the jump of an atom in a supercell containing N atoms by considering the constraint

$$g_{B_j}(\{\mathbf{r}_i\}_{i=1,N}) = \mathbf{r}_j\cdot\mathbf{d} - \sum_{\substack{i=1\\ i\neq j}}^{N}\frac{\mathbf{r}_i\cdot\mathbf{d}}{N-1} - C_{B_j} = 0 \tag{6}$$

Here the "gate" is formed by all the atoms except the jumping one. C_{B_j} is a constant. The direction **d**, which in the original proposal was natural to choose as a high symmetry direction, can be chosen arbitrarily; varying this choice allows to explore different valleys, if available.

If we consider the vector in $3N$ dimensions $\bar{\mathbf{X}}_{B_j} = \{B^j_i\}_{i=1,N}$ where:

$$\mathbf{B}^j_i = \begin{cases} -\frac{\mathbf{d}}{N-1} & \forall i \neq j \\ \mathbf{d} & i = j \end{cases} \tag{7}$$

then the constraint in (6) can be rewritten using $3N$ vectors as:

$$g_{B_j}(\overline{\mathbf{X}}) = \overline{\mathbf{X}}\cdot\overline{\mathbf{X}}_{B_j} - C_{B_j} = 0 \tag{8}$$

Another possible constraint, very commonly used, is what defines the so called "drag method". In this case, knowing the initial and final state, defined by $3N$ coordinates, $\overline{\mathbf{X}}^I$ and $\overline{\mathbf{X}}^F$, one can constrain a generic position $\overline{\mathbf{X}}$ in $3N$ dimensions by

$$g_{drag}(\overline{\mathbf{X}}) = \overline{\mathbf{X}}\cdot\overline{\mathbf{X}}_D - C_D = 0 \tag{9}$$

where $\overline{\mathbf{X}}_D = \overline{\mathbf{X}}^F - \overline{\mathbf{X}}^I$ and C_D is a constant.

From Eqs. (9) and (8) one can see that the two constraints have the same form. In order to find a migration path one has to perform several constrained relaxations, each step m ($m = 1, M$) being defined by the value of the constant, C_D or C_{B_j}. In both cases one can express the constant as a scalar product, $\overline{\mathbf{X}}^m\cdot\overline{\mathbf{X}}_D$ or $\overline{\mathbf{X}}^m\cdot\overline{\mathbf{X}}_{B_j}$; for the drag method the natural choice is:

$$\overline{\mathbf{X}}^m = \overline{\mathbf{X}}^I + \frac{m}{M}(\overline{\mathbf{X}}^F - \overline{\mathbf{X}}^I) \tag{10}$$

while for the Bennett-like constraint we used:

$$\overline{\mathbf{X}}^m = \overline{\mathbf{X}}^I + \frac{m}{M}\delta_{ij}\mathbf{d} \tag{11}$$

In practice, $\overline{\mathbf{X}}^m$ was our starting atomic configuration for the mth constrained relaxation.

It can be easily seen that the generalisation of the Bennett constraint (Eq. (8)) reduces to the drag one when the initial and final positions of all the atoms except the jumping one are the same.

The advantage of the starting point (11) is that it is not necessary to know the final position. A further refinement is possible, and is sometimes necessary in order to follow tortous valleys in the energy landscape; this consist in choosing, instead of (11), the following:

$$\overline{\mathbf{X}}^m = \overline{\mathbf{X}}^{m-1}_f + \frac{1}{M}\delta_{ij}\mathbf{d} \tag{12}$$

where we noted by $\overline{\mathbf{X}}^{m-1}_f$ the final position of the previous constrained relaxation of the series. We have verified in several cases that this choice makes the path search almost insensitive to the direction **d** on which the jumping atom, j, is pushed. A similar choice consists in taking:

$$\overline{\mathbf{X}}^m = \overline{\mathbf{X}}^{m-1}_f + \alpha\left(\overline{\mathbf{X}}^{m-1}_f - \overline{\mathbf{X}}^{m-2}_f\right) \tag{13}$$

where α fixes the relative size of successive steps.

The constraint (6) is implemented in the PWSCF code, part of the Quantum-Espresso suite [22].

References

[1] T. Yano, H. Miyazaki, M. Akiyoshi, T. Iseki, J. Nucl. Mater. 253 (1998) 78.
[2] Y. Katoh, N. Hashimoto, S. Kondo, L.L. Snead, A. Kohyama, J. Nucl. Mater. 351 (2006) 228–240.
[3] M. Bockstedte, A. Mattausch, O. Pankratov, Phys. Rev. B 68 (2003) 205201.
[4] A. Mattausch, M. Bockstedte, O. Pankratov, Phys. Rev. B 70 (2004) 235211.
[5] T. Lingner, S. Greulich-Weber, J.M. Spaeth, U. Gerstmann, E. Rauls, Z. Hajnal, T. Frauenheim, H. Overhof, Phys. Rev. B 64 (2001) 245212.
[6] M. Bockstedte, A. Mattausch, O. Pankratov, Phys. Rev. B 69 (2004) 235202.
[7] U. Gerstmann, E. Rauls, H. Overhof, Phys. Rev. B 70 (2004) 201204.
[8] C. Fu, J. Dalla Torre, F. Willaime, J. Bocquet, A. Barbu, Nat. Mater. 4 (1) (2005) 68–74.
[9] R.R. Hart, H.L. Dunlap, O.J. March, Radiat. Effects 9 (1971) 261–266.
[10] M. Ishimaru, I.-T. Bae, Y. Hirotsu, S. Matsumura, K.E. Sickafus, Phys. Rev. Lett. 89 (2002) 055502.
[11] M. Ishimaru, I.-T. Bae, Y. Hirotsu, Phys. Rev. B 68 (2003) 144102.
[12] R. Devanathan, F. Gao, W.J. Weber, Appl. Phys. Lett. 84 (2004) 3909.
[13] L. Malerba, J.M. Perlado, Phys. Rev. B 65 (2002) 045202.
[14] F. Gao, W.J. Weber, J. Appl. Phys. 94 (2003) 4348.
[15] E. Rauls, T.E.M. Staab, Z. Hajnal, T. Frauenheim, Physica B 308–310 (2001) 645.
[16] A. Gali, P. Deák, P. Ordejón, N.T. Son, E. Janzén, W.J. Choyke, Phys. Rev. B 68 (2003) 125201.
[17] T. Hornos, N.T. Son, E. Janzén, A. Gali, Phys. Rev. B 76 (2007) 165209.
[18] G. Lucas, L. Pizzagalli, J. Phys. Condens. Matter 19 (2007) 086208.
[19] N.T. Son, E. Janzén, J. Isoya, N. Morishita, H. Hanaya, H. Takizawa, T. Ohshima, A. Gali, Phys. Rev. B 80 (2009) 125201.
[20] E. Kotomin, V. Kuzovkov, Rep. Prog. Phys. 55 (1992) 2079–2188.
[21] T. Liao, G. Roma, J. Wang, Philos. Mag. 89 (2009) 2271–2284.
[22] P. Giannozzi, S. Baroni, N. Bonini, M. Calandra, R. Car, C. Cavazzoni, D. Ceresoli, G. Chiarotti, M. Cococcioni, I. Dabo, A.D. Corso, S. Fabris, G. Fratesi, S. de Gironcoli, R. Gebauer, U. Gerstmann, C. Gougoussis, A. Kokalj, M. Lazzeri, L. Martin-Samos, N. Marzari, F. Mauri, R. Mazzarello, S. Paolini, A. Pasquarello, L. Paulatto, C. Sbraccia, S. Scandolo, G. Sclauzero, A.P. Seitsonen, A. Smogunov, P. Umari, R.M. Wentzcovitch, J. Phys. Condens. Matter 21 (2009) 39.
[23] G. Henkelman, B.P. Uberuaga, H. Jónsson, J. Chem. Phys. 113 (2000) 9901.
[24] C.H. Bennett, Diffusion in Solids: Recent Developments, Academic Press, New York, 1975. p. 73.
[25] T.A.G. Eberlein, R. Jones, S. Öberg, O.R. Briddon, Phys. Rev. B 74 (2006) 144106.
[26] F. Gao, J. Du, E.J. Bylaska, M. Posselt, W.J. Weber, Appl. Phys. Lett. 90 (2007) 221915.
[27] G.L. Zhao, D. Bagayoko, T.D. Williams, Phys. Rev. B 60 (1999) 1563.
[28] G. Lucas, L. Pizzagalli, Phys. Rev. B 72 (2005) 161202.
[29] A.A. Lebedev, A.I. Veinger, D.V. Davydov, V.V. Kozlovski, N.S. Savkina, A.M. Strel'chuk, J. Appl. Phys. 88 (2000) 6265.
[30] T.R. Waite, J. Chem. Phys. 32 (1960) 21.
[31] J.C. Bourgoin, J.W. Corbett, Radiat. Effects 36 (1978) 157–188.
[32] J.W. Steeds, W. Sullivan, A. Wotherspoon, J.M. Hayes, J. Phys. Condens. Matter 21 (2009) 364219.